

KINETICS OF THE REACTION BETWEEN H· AND SUPERHEATED WATER PROBED WITH MUONIUM

C. Alcorn¹, J.-C. Brodovitch², K. Ghandi*¹, A. Kennedy¹, P.W. Percival*^{2,3}, M. Smith¹

¹Mount Allison University, Sackville, New Brunswick, Canada

²Simon Fraser University, Burnaby, British Columbia, Canada

³TRIUMF, Vancouver, British Columbia, Canada

Abstract

Safe operation of a supercritical water cooled reactor requires knowledge of the reaction kinetics of transient species formed by the radiolysis of water in the temperature range 300–650°C. By using a light isotope of the H-atom, it is possible to study its chemistry in water over this range of temperatures. Arguably, the most important reaction to study is that of the H-atom with the bulk solvent. This reaction could provide an *in situ* source of H₂ gas, which is added to CANDU reactors to suppress oxidative corrosion. The work described here concerns studies of the reaction of muonium with H₂O and D₂O at temperatures up to 450°C.

1. Introduction

Supercritical water (SCW) has widespread potential as a replacement for solvents in common use today because is a “tunable” solvent, meaning that near the critical point small changes in temperature and pressure can widely vary intrinsic properties such as density, viscosity, dielectric constant and degree of hydrogen bonding [1]. In practice, this means a wide range of solvent properties are accessible by changing the thermodynamic conditions.

SCW is currently used in industrial applications, of which two examples are supercritical water oxidation (SCWO) for hazardous waste destruction [2] and materials processing and chemical synthesis (aquathermolysis) [3]. Our present study is motivated by the potential to use SCW in the next generation (Gen IV) SCW-cooled nuclear reactors (SCWRs) [4], for example, the CANDU SCWR, which utilize sub-critical heavy water as the neutron moderator and SCW as the coolant.

Modeling of aqueous chemistry in the heat transport systems of pressurized-water-cooled reactors and SCWRs is required to determine the concentrations of the species that are produced from radiolysis of water, in particular those that may cause corrosion of materials that might be used in the reactors. The modeling of radiolysis requires accurate data on the rate constants of reactions involved in the radiolysis of water (e.g. H₂O⁺, H₂O^{*}, H₂O⁻, OH, H· [5]), and rate constants of reactions of potential additives used to control water chemistry under extreme conditions. Unfortunately, most experimental data sets do not even extend to the temperatures used in current reactors, well short of the supercritical conditions envisaged in Gen IV designs. Thus, a major technology gap for SCWR development is the lack of knowledge of radiolysis of water under supercritical conditions. We have initiated a project to explore chemical kinetics in this regime, with an initial focus on the range of 320°C to 450°C.

Arguably, one of the most important reactions in the suppression of net water radiolysis is the equilibrium reaction between $\text{H}\cdot$ and water itself:



The forward reaction is known to produce molecular hydrogen in the gas phase [6], and it is thought to be responsible for the increase in the g-value of H_2 observed in pulse radiolysis in high temperature water [7-9]. This is of interest because molecular hydrogen is added to the coolant in current nuclear reactors to suppress water decomposition and O_2 production [5], and this reaction could produce molecular hydrogen *in situ* and thereby sustain or enhance the amount of added hydrogen. However, due to the increased stability of charged species in solution at intermediate temperatures, in particular under subcritical conditions, there may be a shift of this reaction from hydrogen-producing to electron-producing:



A controversy currently exists in the literature regarding the forward rate constant of reaction (1) under hydrothermal conditions [7-9]. Uncertainties arise from the lack of data on solvation energies of transient species under supercritical conditions. Estimates of reaction rates were based on assuming that the ratio $\Delta G_{\text{hyd}}(\text{H}_2\text{O})/\Delta G_{\text{hyd}}(\cdot\text{OH})$ is analogous to the known ratio $\Delta G_{\text{hyd}}(\text{H}_2\text{O}_2)/\Delta G_{\text{hyd}}(\text{H}_2\text{O})$, based on their abilities to form hydrogen bonds [8]. However there are different opinions on the temperature dependence of $\Delta G_{\text{hyd}}(\cdot\text{OH})$ [9]. For high temperature water (300°C) Bartels estimates the upper limit of the abstraction rate constant to be $6.1 \times 10^3 \text{ M}^{-1}\text{s}^{-1}$, while Swiatla-Wojcik estimates the rate constant to be $1.8 \times 10^4 \text{ M}^{-1}\text{s}^{-1}$. Since these calculations find the rate constant by assuming an equilibrium between the forward and reverse reactions such that

$$\frac{k_f}{k_r} = K = e^{\left[\frac{-\Delta G_{\text{rxn}}}{RT}\right]} \quad (3)$$

then both estimates are invalid if the reaction proceeds through an intermediate.

In this work, the reaction $\text{H}\cdot + \text{H}_2\text{O}$ is investigated using muonium ($\text{Mu}\cdot$) as an analogue of a hydrogen atom. $\text{Mu}\cdot$ is an exotic atom, with an unstable positive muon (μ^+ , 2.2 μs lifetime, mass ~ 0.11 amu) as the nucleus [10-12]. Because the reduced mass of $\text{Mu}\cdot$ and $\text{H}\cdot$ are nearly the same, (the reduced mass of muonium is 99.5% that of hydrogen) $\text{Mu}\cdot$ is considered a light isotope of $\text{H}\cdot$ and reacts similarly to $\text{H}\cdot$. The reactions of $\text{Mu}\cdot$ with H_2O and D_2O were studied from sub- to supercritical conditions, extending earlier work [13,14] to 450°C and 300 bar.

2. Experimental Details

The H_2O used was distilled, or distilled deionized water. D_2O (Cambridge Isotope Laboratories, Inc. 99.9% D) was used without further purification. Dissolved oxygen was removed from our samples by the “pump-shake” method: the liquid sample is repeatedly pressurized with argon,

shaken, and vacuum pumped. Five to six cycles of this procedure were performed on each sample, after which they were stored in glass bulbs under ~2 bar argon, which aids in the transfer of the sample into the target cell.

The μ SR experiments were carried out at TRIUMF in Vancouver, BC, Canada, using the M9B muon beam-line. The beam momentum was adjusted such that the muons passed through the window of a pressure vessel and stopped in the fluid sample. The beam is highly spin-polarized (~80%) and a weak magnetic field (~5 gauss) was applied transverse to the muon spin direction, so that the stopped muons precessed at frequencies characteristic of their chemical environment, in similar fashion to more conventional forms of magnetic resonance spectroscopy. Muons which are incorporated in diamagnetic molecules (MuOH or MuH) spin precess at the muon Larmor frequency, 0.01355 MHz/ G, but those which form muonium have a spin precession frequency in low magnetic field 103 times faster than the diamagnetic fraction. If muonium undergoes a chemical reaction which places the muons in a different magnetic environment, then the resulting spin dephasing is manifest as a decay in the muonium precession signal. The μ SR signal can then be described by

$$S(t) = A_{\text{Mu}} e^{-\lambda_{\text{exp}} t} \cos(\omega_{\text{Mu}} t + \phi_{\text{Mu}}) + A_{\text{D}} \cos(\omega_{\text{D}} t + \phi_{\text{D}}) \quad (4)$$

where t is time, A_{Mu} and A_{D} the amplitudes, ω_{Mu} and ω_{D} the frequencies, and ϕ_{Mu} and ϕ_{D} the initial phases of the muonium and diamagnetic signals. λ_{exp} is the relaxation rate of the muonium signal; the decay of the diamagnetic signal is negligible by comparison. A typical μ SR signal is displayed as Figure 1.

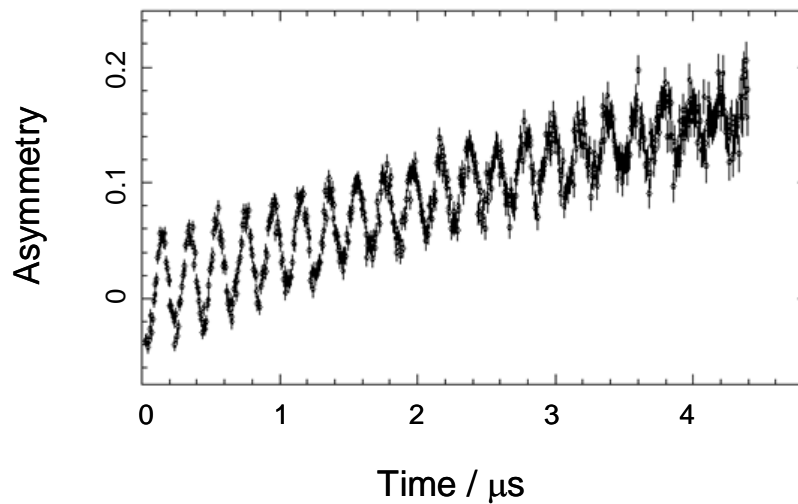


Figure 1 $\text{Mu}\cdot$ in D_2O at 390°C and 250 bar. The fast oscillating signal is due to muon spin precession in muonium in a small transverse magnetic field. The diamagnetic frequency is much smaller and only a fraction of a cycle is visible in this time range.

The “triplet” muonium precession frequency ω_{Mu} is 103 times faster than the diamagnetic muon precession frequency ω_{D} [10-12]. By fitting equation 3 to the μ SR signal it is possible to extract

the exponential decay rate λ_{exp} . Since there is negligible change in reactant concentration over the course of an experiment, muonium kinetics is pseudo-first order:

$$\lambda_{\text{exp}} = \lambda_0 + k_{\text{Mu}} [\text{X}] \quad (5)$$

where k_{Mu} is the rate constant, $[\text{X}]$ the concentration of reactant (in this case H_2O or D_2O), and λ_0 the background relaxation due to field inhomogeneity and the unresolved splitting of the near degenerate precession frequency.

In addition to the background relaxation, further correction is required to account for the self-ionization of water, which results in a temperature- and pressure-dependent concentration of OH^- ions. The magnitude of this effect was estimated from the concentration of OH^- ions produced as a function of temperature and density [15], and the known rate constant for the reaction of $\text{Mu}\cdot$ with OH^- [16].

However, to our knowledge the pK_W of D_2O has only been reported in the literature at the saturation vapour pressure [17-18]. Unfortunately the difference between pK_W of H_2O and D_2O is not a constant, as demonstrated in Figure 2.

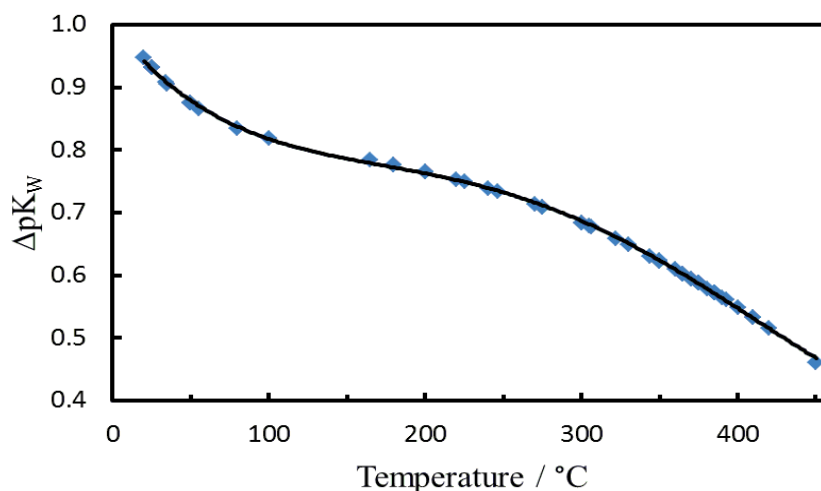


Figure 2 ΔpK_W ($\text{pK}_\text{W}(\text{D}_2\text{O}) - \text{pK}_\text{W}(\text{H}_2\text{O})$) versus temperature at the saturation vapor pressure [17, 18].

Figure 3 shows the pK_W of H_2O and D_2O at the saturation pressure for the densities of the samples investigated in our experiments. It was assumed that the *difference* in pK_W of H_2O and D_2O remains constant as a function of pressure. Thus, the pK_W of D_2O was estimated by first calculating the pK_W of H_2O at the appropriate thermodynamic conditions, and correcting the value by the appropriate factor (Figure 2) as a function of temperature. Figure 4 shows the calculated pK_W of H_2O and D_2O for all thermodynamic conditions in this work, as a function of density.

The rate constant for reaction of $\text{Mu}\cdot$ with OD^- was assumed to be the same as that for reaction with OH^- . While this will introduce some error, it is likely to be negligible since the magnitude of the relaxation due to OH^- is at most 5% of the total observed relaxation.

Applying these corrections, we calculate k_{Mu} from

$$k_{\text{Mu}} = \frac{(\lambda_{\text{exp}} - \lambda_0 - \lambda_{\text{OH}}(T, \rho))}{[\text{X}_0]} \frac{\rho_0}{\rho(T, P)} \quad (6)$$

where λ_{OH} is the relaxation due to reaction of muonium with OH^- from ionization of water, and X_0 and ρ_0 refer to the concentration and density of water at standard temperature and pressure, T is the temperature and P is the pressure. Density as a function of T and P was taken from a NIST database [19-21].

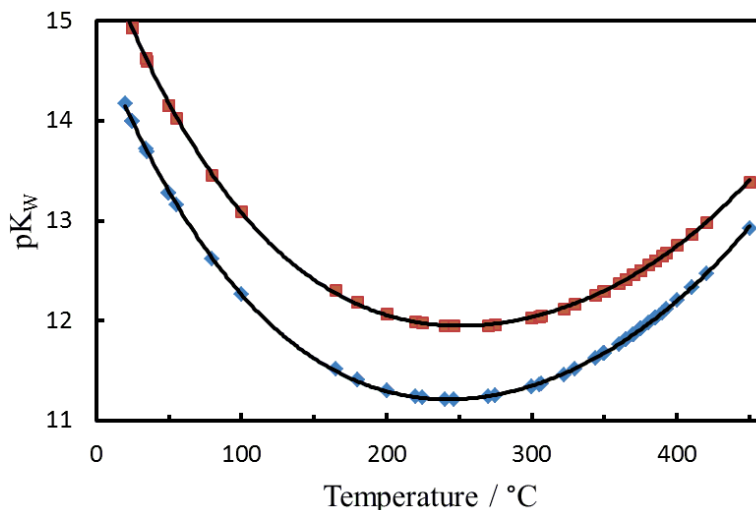


Figure 3 pK_{W} of H_2O (blue diamonds) and D_2O (brown squares) versus temperature along the saturation curve.

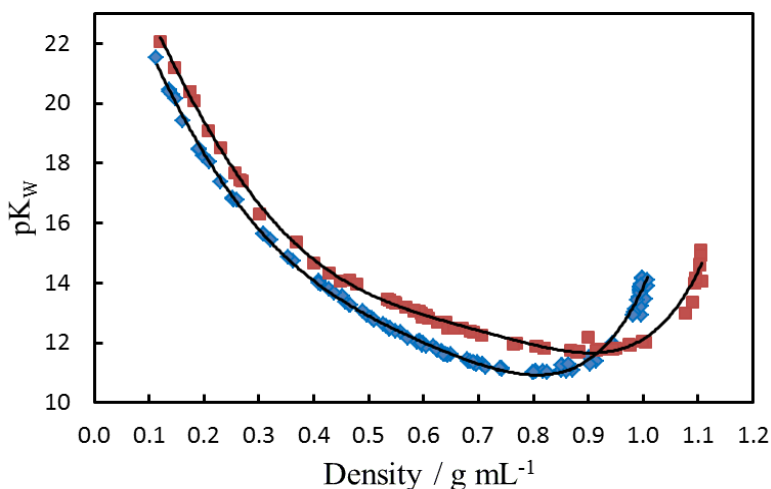


Figure 4 pK_{W} of H_2O (blue diamonds) and D_2O (brown squares) versus density. The best fit is a 5th order polynomial, used to determine the concentration of OH^- ions as a function of density.

The rate constant of $\text{Mu}\cdot + \text{OH}^-$ reaction was fitted to a 4th order polynomial function of density (Figure 5). All fit parameters are presented in the next section.

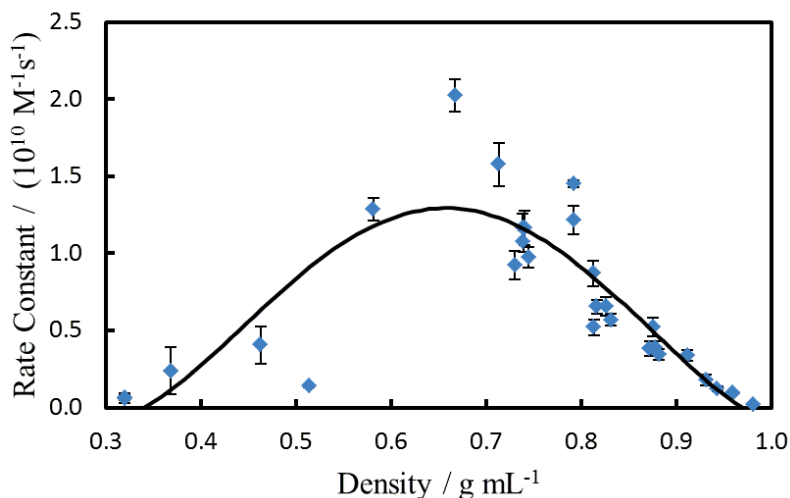


Figure 5 Fit of the rate constants of $\text{Mu}\cdot + \text{OH}^-$ [16] to a polynomial function of density.

3. Experimental Results and Discussion

Data for this work was obtained over several visits to TRIUMF, and during each beam time samples were run with significant overlap of experimental conditions to ensure reproducible results. Even during each run several thermodynamics conditions were repeated to critically evaluate our data set. Where inconsistencies were present, data with the lowest experimental relaxation were used. Inconsistencies could be due to impurities in the water from different sources, and by passivating the reactor vessel at high temperatures for extended periods of time, as well as repeated refills of purified water, we eventually reached what we believe is the most accurate data set. Figures 6 and 7 show our full set of experimental data as a function of density over several runs, along with the fit to the data points with the lowest relaxation rates, which was used for the analysis of the reaction of $\text{Mu}\cdot$ and $\text{H}_2\text{O}/\text{D}_2\text{O}$. The error bars displayed in the plots stem from statistical uncertainties in the μSR data, carried over in the signal fits.

Figure 7 shows the muonium relaxation rates selected as most accurate. Some scatter is seen, especially at lower densities, but this can be attributed to points with different temperature and pressure but the same density, as well as possible effects of near critical fluctuations that, in addition to bulk density, could change the rate of reactions [22]. For example, for H_2O , significant scatter is seen at very low densities, where there is a very large range of pressures (235-300 bar), whereas for D_2O at low densities the pressure range is much smaller (235-250 bar).

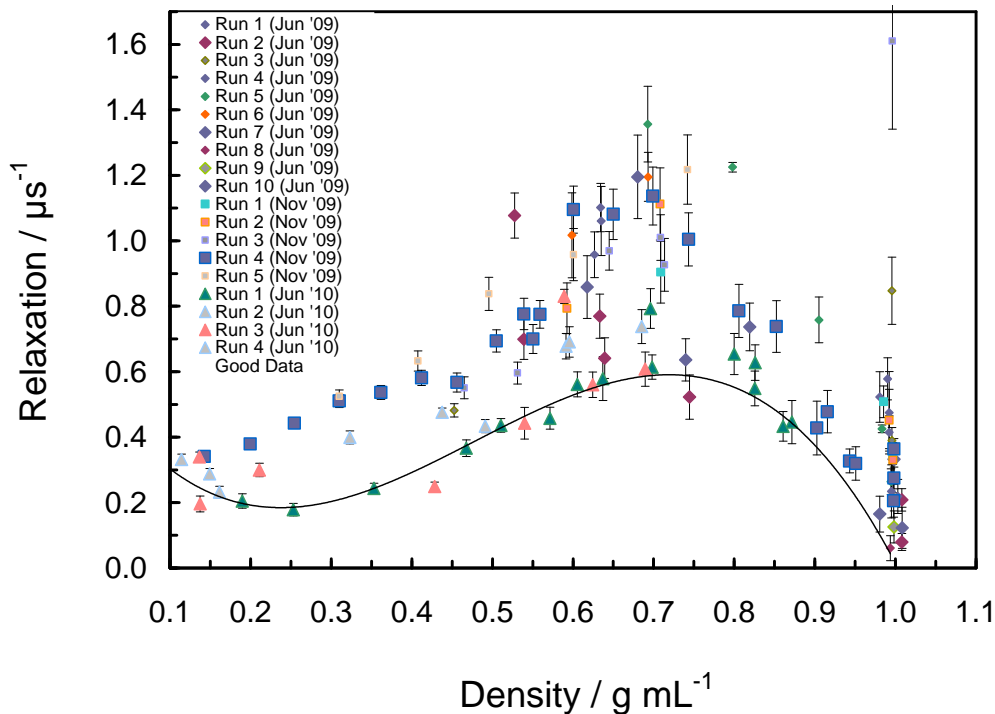


Figure 6 The muonium decay rate in H₂O versus density over all runs. The lowest relaxation data set is shown as a solid line to guide the eyes only.

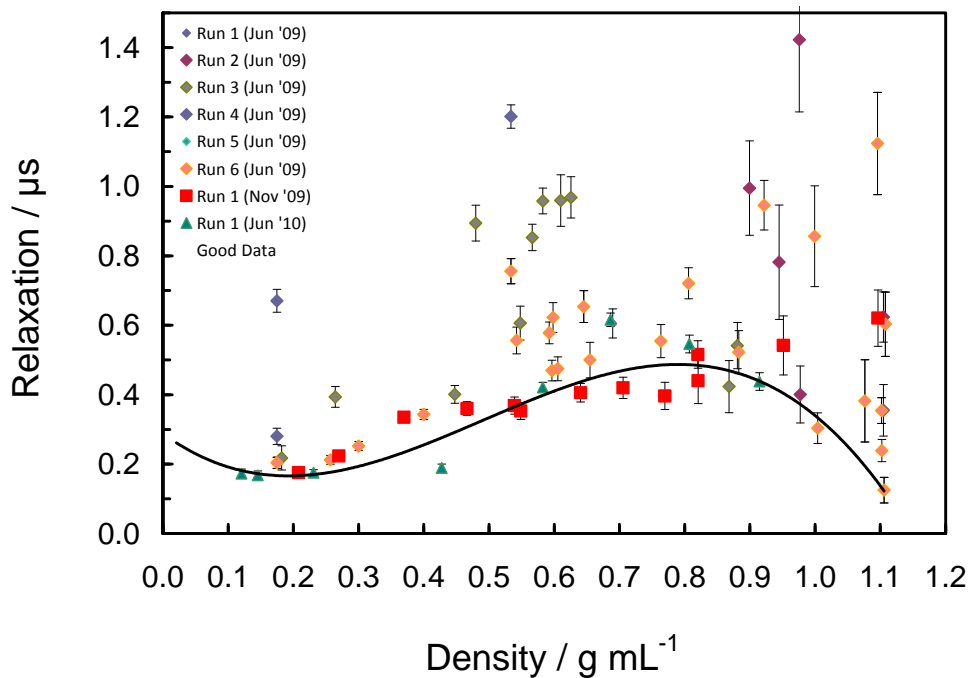


Figure 7 The muonium decay rate in D₂O versus density from all runs. The lowest relaxation data set is shown as a solid line to guide the eyes only.

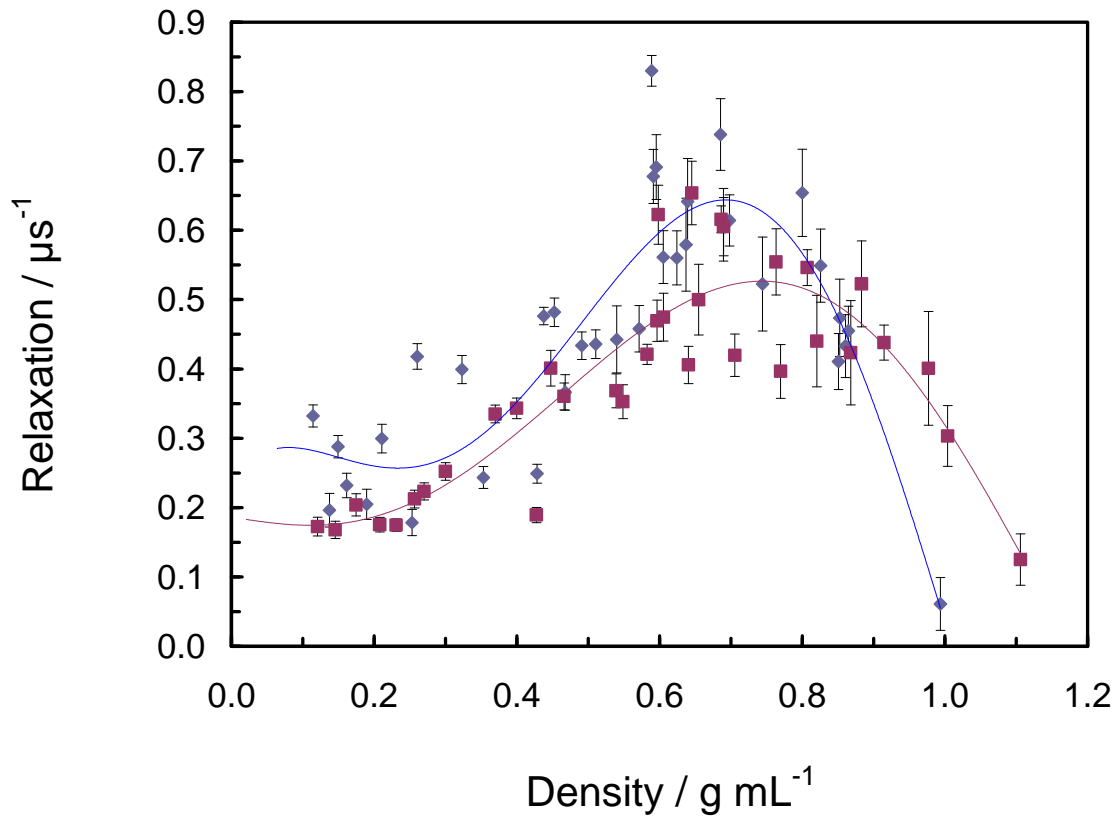


Figure 8 The most accurate muonium decay rates in H₂O (blue diamonds) and D₂O (brown squares) as a function of density. The curves are fits to 5th order polynomials.

From the fits in Figure 8, we are able to express the experimental relaxation rates as a power series in density, as shown in equation 7

$$\lambda_{\text{exp}}(\rho) = c_5\rho^5 + c_4\rho^4 + c_3\rho^3 + c_2\rho^2 + c_1\rho + c_0 \quad (7)$$

where c_0 to c_5 are fit parameters with different values for H₂O and D₂O, and are listed in Table 1.

Table 1: Parameters obtained by fitting equation 7 to the Mu relaxation data of Figure 8.

Parameter	Value (H ₂ O)	Value (D ₂ O)
$c_5 / \mu\text{s}^{-1}\cdot(\text{g/mL})^{-5}$	26.522	3.882
$c_4 / \mu\text{s}^{-1}\cdot(\text{g/mL})^{-4}$	-73.512	-10.258
$c_3 / \mu\text{s}^{-1}\cdot(\text{g/mL})^{-3}$	68.674	6.885
$c_2 / \mu\text{s}^{-1}\cdot(\text{g/mL})^{-2}$	-25.851	-0.225
$c_1 / \mu\text{s}^{-1}\cdot(\text{g/mL})^{-1}$	4.179	-0.151
$c_0 / \mu\text{s}^{-1}$	0.028	0.186

To obtain values of the rate constant, equation 7 is substituted into equation 6. Similarly, an empirical equation is used to describe the density dependence of λ_{OH} :

$$\lambda_{\text{OH}}(\rho) = a_6\rho^6 + a_5\rho^5 + a_4\rho^4 + a_3\rho^3 + a_2\rho^2 + a_1\rho + a_0 \quad (8)$$

where λ_{OH} is $k_{\text{OH}^-}(\rho)[\text{OH}^-]$ or $k_{\text{OH}^-}(\rho)[\text{OD}^-]$, and where $[\text{OH}^-]$ and $[\text{OD}^-]$ are extracted from the empirical fits shown in Figure 4. The parameters a_6 to a_0 are listed in Table 2 for H₂O and D₂O.

Table 2: Fit parameters of equation 8 for λ_{OH} in H₂O and D₂O

Parameter	Value (H ₂ O)	Value (D ₂ O)
$a_6 / \mu\text{s}^{-1}\cdot(\text{g/mL})^{-6}$	10.076	2.0573
$a_5 / \mu\text{s}^{-1}\cdot(\text{g/mL})^{-5}$	-27.131	-6.741
$a_4 / \mu\text{s}^{-1}\cdot(\text{g/mL})^{-4}$	25.78	8.4295
$a_3 / \mu\text{s}^{-1}\cdot(\text{g/mL})^{-3}$	-10.337	-5.1581
$a_2 / \mu\text{s}^{-1}\cdot(\text{g/mL})^{-2}$	1.7049	1.6307
$a_1 / \mu\text{s}^{-1}\cdot(\text{g/mL})^{-1}$	-0.0934	-0.2262
$a_0 / \mu\text{s}^{-1}$	0.0001	0.0108

The resulting rate constants as a function of density are shown in Figure 9.

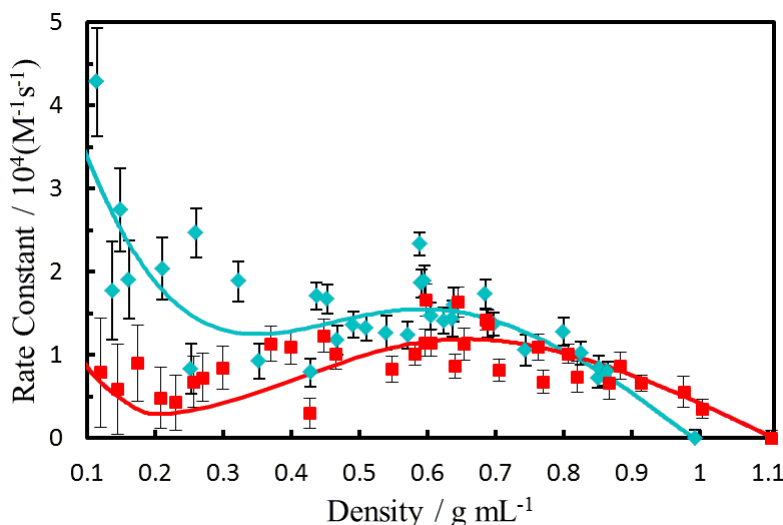


Figure 9 Rate constants of $\text{Mu}\cdot + \text{H}_2\text{O}$ (blue line from equation 8) and $\text{Mu}\cdot + \text{D}_2\text{O}$ (red line from equation 8) along with our experimental data (H₂O blue diamonds, D₂O red squares).

4. Conclusions

We have experimentally determined rate constants for the reactions $\text{Mu}\cdot + \text{H}_2\text{O}$ and $\text{Mu}\cdot + \text{D}_2\text{O}$ up to 450°C. A fit to our experimental data has been performed taking into account density as the main parameter affecting rate constants, showing reasonable predictions of rate constants up to $\rho \sim 0.7 \text{ g/mL}$, with significant scatter seen at lower densities. This scatter stems from identical densities obtained under significantly different thermodynamic conditions, as well as possible effects of near critical fluctuations.

Immediate future plans for this project include fitting the data to theoretical models involving quantifying these critical fluctuations, and since this phenomenon depends on properties of the solvent, the models would be of benefit in describing the effects of thermodynamic conditions for *any* reaction in near critical water. *Ab initio* calculations are required to explain the mechanism and thermodynamics of this reaction. Since significant kinetic isotope effects can exist when considering $\text{Mu}\cdot$ as a probe for H· atom reactions, such effects should be investigated.

It is also of great value to the Gen IV SCWR community to extend the temperature range of the experimental data for $\text{H}\cdot + \text{H}_2\text{O}$ to much higher temperatures, because Gen IV designers are currently planning core exit temperatures as high as 650°C. μSR methods will be able to reach these temperatures in the very near future with the commission of a new cell, and so the uncertainties surrounding this reaction beyond 450°C can be resolved.

5. Acknowledgements

We thank Dr. Syd Kreitzman and the staff of the TRIUMF μSR facility for technical support. This research was financially supported by the Natural Sciences and Engineering Research Council of Canada and Natural Resources Canada (NRCAN), and through TRIUMF by the National Research Council of Canada. Their support is gratefully acknowledged. Special thanks go to Palak Satija, Emma Driedger and Mina Mozafari for help on taking data at TRIUMF.

6. References

- [1] Weingartner, H.; Franck, E. U. *Angew. Chem. Int. Ed.* 2005, 44, 2672–2692.
- [2] Bermejo, M. D.; Cocero, M. J. *AIChE Journal* 2006, 52, 3933-3951.
- [3] Katritzky, A. R.; Allin, S. M.; Siskin, M. *Acc. Chem. Res.* 1996, 29, 399-406.
- [4] Khartabil, H. *GIF Symposium, Paris (France), 9-10 September, 2009.*
- [5] Lin, C. C.; Radiochemistry in Nuclear Power Reactors, Washington D.C.: National Academy Press, 1996.
- [6] Micheal, J. V.; Sutherland, J. W. *J. Phys. Chem.* 1988, 92, 3853-3857.
- [7] Swiatla-Wojcik, D.; Buxton, G. V. *Radiation Physics and Chemistry* 2005, 74, 210–219.
- [8] Bartels, D. *Radiation Physics and Chemistry* 2009, 78, 191–194.
- [9] Swiatla-Wojcik, D.; Buxton, G. V. *Radiation Physics and Chemistry* 2010, 79, 52–56.
- [10] Cox, S. F. J. *J. Phys. C: Solid State Phys.* 1987, 20, 3187-3319.

- [11] Walker, D. C. *J. Chem. Soc., Faraday Trans.* 1998, 94, 1-9.
- [12] Roduner, E.; McKenzie, I. *Naturwissenschaften* 2009, 96, 873–887.
- [13] Percival, P. W.; Brodovitch, J. C.; Ghandi, K.; Addison-Jones, B.; Schüth, J.; Bartels, D. M. *Phys. Chem. Chem. Phys.* 1999, 1, 4999-5004.
- [14] Ghandi, K.; Brodovitch, J. C.; Addison-Jones, B.; Brodovitch, J. C.; Percival, P. W.; Schüth, J. *Physica B* 2000, 289-290, 476-481.
- [15] Marshall, W. L.; Franck, E. U. *J. Phys. Chem. Ref. Data* 1981, 295-304.
- [16] Ghandi, K.; Addison-Jones, B.; Brodovitch, J. C.; Kecman, S.; McKenzie, I.; Percival, P. W. *Physica B* 2003, 326, 55–60.
- [17] Shoesmith, D. W.; Lee, W. *Can. J. Chem.* 1976, 54, 3553-3558.
- [18] Mesmer, R. E.; Herting, D. L. *Journal of Solution Chemistry* 1978, 12, 901-913.
- [19] Wagner, W.; Pruss, A. *J. Phys. Chem. Ref. Data* 2002, 31, 387-535.
- [20] Saul, A.; Wagner, W. *J. Phys. Chem. Ref. Data* 1989, 18, 1537-1564.
- [21] IAPWS, Revised Release on the IAPS Formulation 1985 for the Viscosity of Ordinary Water Substance, International Association for the Properties of Water and Steam, Erlangen, Germany, 1997, 15.
- [22] Tucker, S. C. *Chem. Rev.* 1999, 99, 391-418.